## SPIN-SHAPE MODEL FOR 357 NININA

Lorenzo Franco
Balzaretto Observatory (A81), Rome, ITALY
lor_franco@libero.it

Frederick Pilcher
Organ Mesa Observatory (G50)
4438 Organ Mesa Loop
Las Cruces, NM 88011 USA

Julian Oey
Blue Mountains Observatory (Q68)
94 Rawson Pde. Leura, NSW, AUSTRALIA

Alessandro Marchini, Riccardo Papini
Astronomical Observatory, University of Siena (K54)
Via Roma 56, 53100 - Siena, ITALY

Giulio Scarfi
Iota Scorpii Observatory (K78), La Spezia, ITALY

Marco Iozzi
HOB Astronomical Observatory (L63)
Capraia Fiorentina, ITALY

Nello Ruocco
Osservatorio Astronomico Nastro Verde (C82)
Sorrento, ITALY

Paolo Bacci, Martina Maestripieri
GAMP - San Marcello Pistoiese (104), Pistoia, ITALY

Nico Montigiani, Massimiliano Mannucci
Osservatorio Astronomico Margherita Hack (A57)
Florence, ITALY

(Received: 2023 November 28)

We present a shape and spin axis model for main-belt asteroid 357 Ninina. The model was achieved with the lightcurve inversion process, using combined dense photometric data acquired from five apparitions between 2007-2023 and sparse data from USNO Flagstaff. Analysis of the resulting data found a sidereal period P = 35.9840 ± 0.0005 hours and two mirrored pole solutions at (λ = 49°, β = 0°) and (λ = 230°, β = 36°) with an uncertainty of ± 10 degrees.

The minor planet 357 Ninina was observed by the authors for five oppositions from 2007 to 2023 and, to improve the coverage at various aspect angles, we also used the sparse data from USNO Flagstaff Station, according Durech et al. (2009). Most of the dense data were downloaded from ALCDEF (ALCDEF, 2021) and sparse data from the Asteroids Dynamic Site (AstDyS-2, 2020).

The observational details of the dense data used are reported in Table I with the reference, the mid-date, number of the lightcurves used for the inversion process, longitude and latitude of phase angle bisector (LPAB, BPAB). The dense data points were binned in sets of 5 with maximum time difference 5 minutes, in order to reduce the overall processing time. The PAB longitude/latitude distribution of the dense and sparse data are shown on Figure 1, while Figure 2 shows the phase curve obtained with the sparse data.

| # | Reference | Mid-date | # LC | LPAB | BPAB |
|---|---|---|---|---|---|
| 1 | Oey (2014) | 2007-07-27 | 8 | 310 | 3 |
| 2 | Oey (2008) (*) | 2008-10-10 | 3 | 39 | 18 |
| 3 | Oey (2014) | 2013-09-15 | 17 | 343 | -9 |
| 4 | Pilcher (2021) | 2021-01-10 | 16 | 112 | -8 |
| 5 | Pilcher (2023) | 2023-05-30 | 18 | 251 | 17 |

Table I. Observational details for the dense data used in the lightcurve inversion process for 357 Ninina.
(*) Item 2 published only on 'alcdef.org' web site.

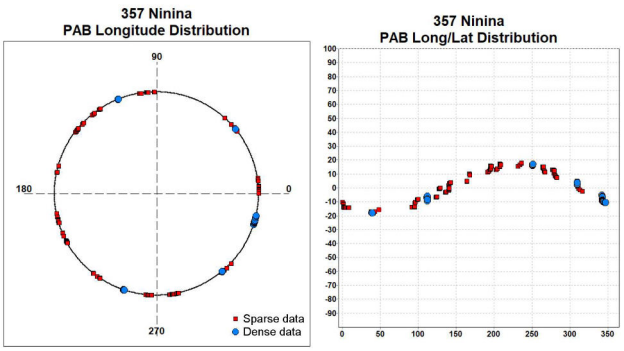


Figure 1: PAB longitude/latitude distribution for the dense and sparse data used in the lightcurve inversion process.

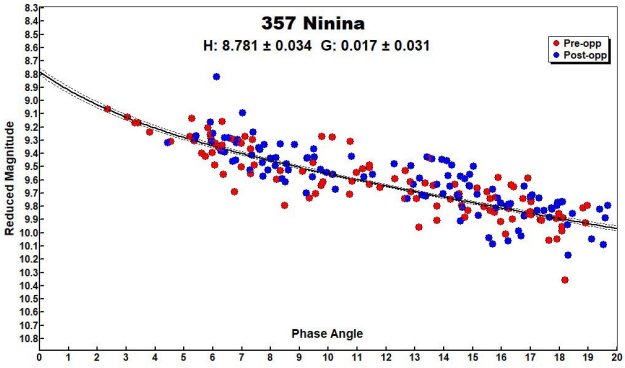


Figure 2: Phase curve obtained from sparse data (reduced magnitude vs phase angle).

Lightcurve inversion was performed using MPO LCInvert v.11.8.4.1 (MPO LCInvert, 2022). For a description of the modeling process see LCInvert Operating Instructions Manual, Durech et al. (2010); and references therein.

In the analysis the processing weighting factor was set, according the data quality of the single dataset, to: 1.0 [#4, #5]; 0.9 [#1, #3]; 0.4 [#2] for dense data and 0.3 for sparse data. The "dark facet" weighting factor was set to 0.5 to keep the dark facet area below 1% of total area and the number of iterations was set to 50.

In lightcurve inversion work, the most critical step is to find an accurate sidereal rotation period. An inaccurate sidereal period can lead to completely incorrect results, regarding the spin axis and the model.

The period search scan was started around 3-sigma interval centered on the average of the synodic periods relative to the dense data used for the inversion process. We found one well isolated sidereal period with a Chi-Sq below to the 9% limit for P=35.9842 h (Figure 3).

In order to verify this result, we plotted the observed synodic periods versus daily change rate of the phase angle bisector longitude (Figure 4). In this plot the intercept of the regression line with the stationary point (ΔPABL/day=0) represents the sidereal period. We found a value of the intercept (35.9814 ± 0.0105 h), consistent with the sidereal period found through the period search scan step (35.9842 h.) and this positive verification reassures us for the subsequent pole searching step. Moreover, the increasing trend of the regression line suggest a prograde rotation.

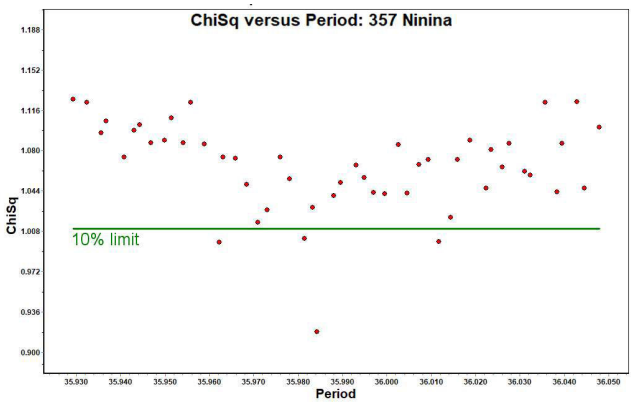


Figure 3: The period scan for 357 Ninina shows one isolated sidereal period with a Chi-Sq below to the 9% limit for P=35.9842 h.

| Date (from-to) | PAB_L/day | Syn Period (h) | Period Err (h) |
|---|---|---|---|
| 2007-07-13 – 2007-08-11 | -0.00395 | 35.9640 | 0.0100 |
| 2013-07-24 – 2013-11-14 | 0.07205 | 36.0105 | 0.0001 |
| 2020-12-07 – 2021-02-13 | 0.01360 | 35.9840 | 0.0010 |
| 2023-05-03 – 2023-06-26 | -0.00055 | 36.0000 | 0.0100 |

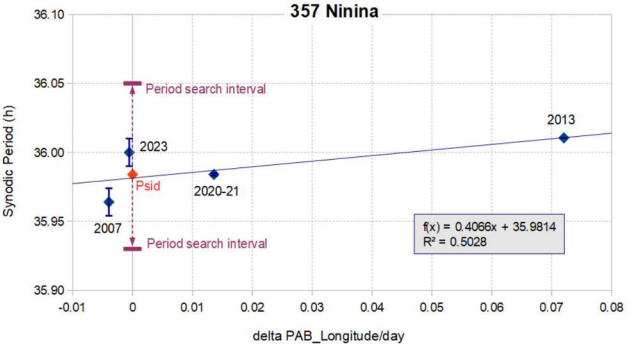


Figure 4: The observed synodic periods versus daily change rate of the phase angle bisector longitude. The synodic period was recalculated for the 2007 data and it is a bit different from published one. The two horizontal bars indicate the interval used for the period search scan. The intercept of the stationary point (ΔPABL/day=0) with the regression line at 35.9814 ± 0.0105 h is consistent with the sidereal period (35.9842 h) found from the period scan step (red point). The increasing trend suggest a prograde rotation.

The pole search was started using the "medium" search option (312 fixed pole position with 15° longitude-latitude steps) and the previously found sidereal period set to "float". From this step we found two roughly mirrored solution with lower Chi-Sq (Figure 5) separated by 180° in longitude, close to ecliptic longitude-latitude pairs (45°, 0°) and (225°, 30°).

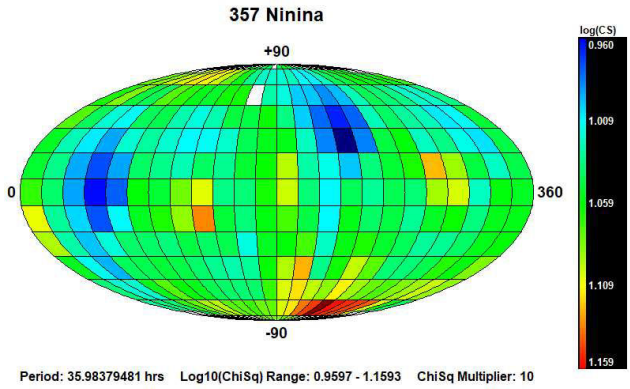


Figure 5: Pole distribution produced by the "medium" search option. The dark blue region indicates the smallest Chi-Sq value while the dark red region indicates the largest. The two roughly mirrored pole solution are approximately centered close to (45°, 0°) and (225°, 30°) with a radius of 30°.

For best focusing the position of the two pole solutions, a "fine" search option (with 49 fixed pole steps with 10° longitude-latitude pairs set to "float") was started with radius of ± 30° on the approximate pole positions found previously. The analysis shows two clustered solutions within 10° of radius that had Chi-Sq values within 10% of the lowest value, approximately centered at ecliptic longitude-latitude (50°, 3°) and (228°, 35°) (Figure 6).

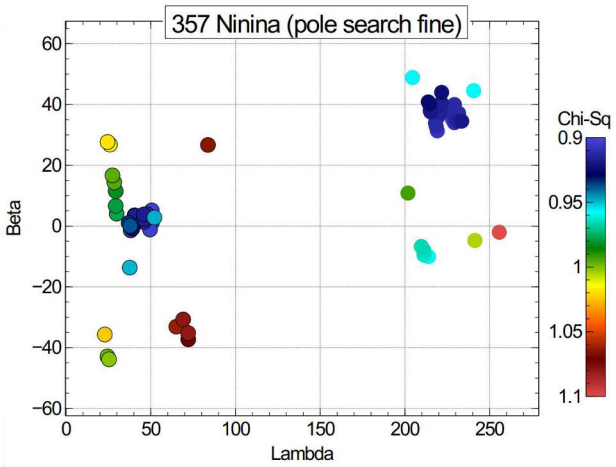


Figure 6: The "fine" pole search shows two clustered solutions (dark blue color) approximately centered near ecliptic longitude-latitude pairs (50°, 3°) and (228°, 35°) with a radius of 10° and Chi-Sq values within 10% of the lowest value.

Moreover, we used the option "none" for refining the two mirrored pole solutions and the relative sidereal periods, found with the previous search option. The two refined solutions are reported in Table II with some statistical data. The reported sidereal period was obtained by averaging the values found into this last step. Typical errors in the pole solution are ± 10° and the uncertainty in sidereal period has been evaluated as a rotational error of 20° over the total time span of the dense data set. We prefer the prograde solution (230°, 36°), consistent with the increasing trend of the regression line on the plot of the synodic periods vs daily change rate PABL.

| λ ° | β ° | Sidereal Period (hours) | RMS | a/b ratio | Ratio of Moments | Angle Phi° |
|---|---|---|---|---|---|---|
| 49 | 0 | 35.9840 ± 0.0005 | 0.0187 | 1.040 | 1.0010 | +5.8 |
| 230 | 36 | | 0.0188 | 1.031 | 1.0003 | +2.6 |

Table II. The two refined spin axis solutions for 357 Ninina (ecliptic coordinates) with an uncertainty of ± 10 degrees. The sidereal period was the average of the two solutions found in the pole search process.

Figure 7 shows the shape model while Figure 8 shows the fit between the model (black line) and some observed lightcurves (red points). The fit appears to be good in relation to the very low amplitude of the lightcurves (< 0.12 mag) and the poor quality of some data.

Finally, to check the reliability of the obtained model, we carried out positively some of the tests [1, 4, 5, 6, 8] proposed by Durech et al. (2016) in the section 2.6.

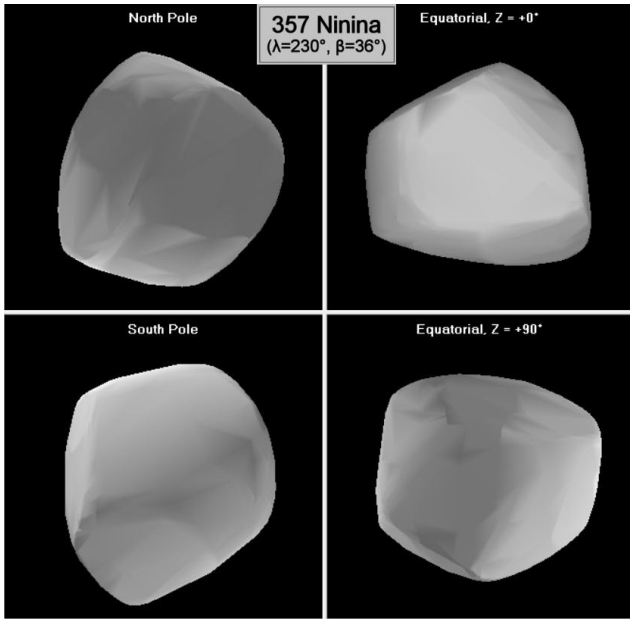


Figure 7: The shape model for 357 Ninina (λ = 230°, β = 36°).

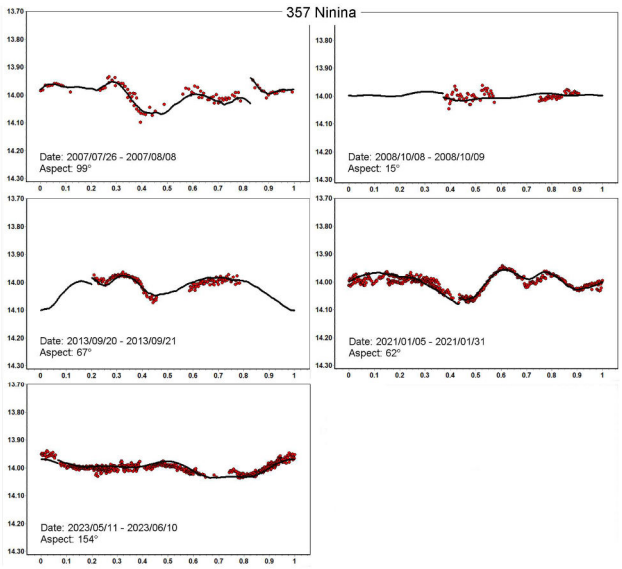


Figure 8: Model fit (black line) versus observed lightcurves (red points) for (λ = 230°, β = 36°) solution.

References

ALCDEF (2021). Asteroid Lightcurve Data Exchange Format web site. *http://www.alcdef.org/*

AstDyS-2 (2020), Asteroids - Dynamic Site. *https://newton.spacedys.com/astdys/*

Durech, J.; Kaasalainen, M.; Warner, B.D.; Fauerbach, M.; Marks, S.A.; Fauvaud, S.; Fauvaud, M.; Vugnon, J.-M.; Pilcher, F.; Bernasconi, L.; Behrend, R. (2009) "Asteroid models from combined sparse and dense photometric data." *A&A* **493**, 291-297.

Durech, J.; Sidorin, V.; Kaasalainen, M. (2010). "DAMIT: a database of asteroid models." *A&A* **513**, A46.

Durech, J.; Hanus, J.; Oszkiewicz, D.; Vanco, R. (2016). "Asteroid models from Lowell photometric database." *A&A* **587**, A48, 1-6.

MPO LCInvert (2022). *https://minplanobs.org/BdwPub/php/mpolcinvert.php*

Oey, J. (2014). "Lightcurve Analysis of Asteroids from Blue Mountains Observatory in 2013." *Minor Planet Bulletin* **41**, 276-281.

Pilcher, F.; Franco, L.; Marchini, A.; Oey, J. (2021). "357 Ninina and 748 Simeisa - Two Asteroids with Earth Commensurate Rotation Periods." *Minor Planet Bulletin* **48**, 233-235.

Pilcher, F.; Franco, L.; Marchini, A.; Papini, R.; Scarfi, G.; Iozzi, M.; Ruocco, N.; Bacci, P.; Maestripieri, M.; Montigiani, N.; Mannucci, M. (2023). "A New Lightcurve of 357 Ninina." *Minor Planet Bulletin* **50**, 255-256.